# Experimental Concept Validation of Touchless Electric Potential Sensing using a Pulsed Electron Beam

James D. Walker III *, Julian Hammerl †, and Hanspeter Schaub ‡
*University of Colorado Boulder, Boulder, Colorado 80303*

**Interactions between the charged plasma of the space environment and spacecraft lead to electric charge accumulating on its surface. Methods for remotely measuring an object's electric potential have been explored and experimentally validated in vacuum chamber conditions. To use these methods however, an additional current is applied to the target by a continuously emitting electron beam, altering the potential of the target. Pulsing has been proposed to reduce the net current applied to the target. In this paper, the use of a pulsed beam for the secondary electron method is experimentally explored in vacuum chamber conditions. To validate the secondary electron method, pulsed beams with duty cycles of 0.1 and 0.01 are used to accurately measure a −500 V potential. A comparison of charging behavior shows that using a pulsed beam has a similar effect as a continuous beam scaled by the duty cycle of the pulsed beam. It is also shown that, for a beam with the same current, a pulsed beam reduces the change in electric potential of the target by more than 90% for multiple beam energies. For this experimental setup, the results of this paper suggest that implementing a pulsed beam is an effective method for remotely sensing a target's potential while minimally perturbing the potential.**

## I. Introduction

Spacecraft charging occurs when the charged plasma of the space environment impacts and accumulates on the surface of the spacecraft[1]. Different regions of space lead to varying levels of charging, even within the same orbit: in a day-side geostationary orbit, the spacecraft will charge to a few volts positive while the same orbit in eclipse can reach negative potentials in the kilo-volt level[1]. Satellites are especially vulnerable to charging in geostationary and cislunar orbits because these regions have a large flux of high energy electrons[1]. These large electrostatic potentials can add risk to docking and proximity operations. As two charged spacecraft approach one another, they exert Coulomb forces and torques that can significantly perturb their relative motion and lead to damaging collisions[2, 3]. Docking operations have an increased risk because Coulomb forces increase inversely with spacecraft separation distance: as the two spacecraft approach each other, the electrostatic perturbations increase exponentially. If the two spacecraft also have different potentials, as they come in contact with one another, arc discharges can damage the electronics of the spacecrafts[3]. Because spacecraft charging already affects current satellites, and, as on-orbit servicing, assembly, and manufacturing activities (OSAM) require greater precision and safety, methods for accounting for and reducing accumulated charge are being developed.

To calculate electrostatic perturbations, a servicing spacecraft must have measurements for electrical charge of the target object, the servicing crafts potential, and the distance between them. To measure its own potential, the spacecraft is equipped with a langmuir probe. These instruments have been proposed for use on spacecraft for measuring plasma density and electron temperature together with the spacecraft potential[4]. Among other methods, LIDAR can be used to measure distance between the two objects in the space environment. While techniques for determining the distance between two objects and the potential of a spacecraft have been explored, methods for remotely sensing the electric potential of a target spacecraft need to be developed. Two methods that have been explored utilize a positively charged servicing spacecraft equipped with a high energy electron beam to excite secondary electrons and x-rays from a target object[5, 6]. The secondary electrons are attracted toward the servicing craft and impact with an energy equal to the difference in electric potential between the two objects while the emitted x-rays have an energy equal to the energy

*Graduate Research Assistant, Ann and H.J. Smead Department of Aerospace Engineering Sciences, Colorado Center for Astrodynamcis Research. James.WalkerIii@colorado.edu

†Graduate Research Assistant, Ann and H.J. Smead Department of Aerospace Engineering Sciences, Colorado Center for Astrodynamcis Research. julian.hammerl@colorado.edu

‡Professor and Department Chair, Schaden Leadership Chair, Ann and H.J. Smead Department of Aerospace Engineering Sciences, Colorado Center for Astrodynamics Research. AAS Fellow, AIAA Fellow

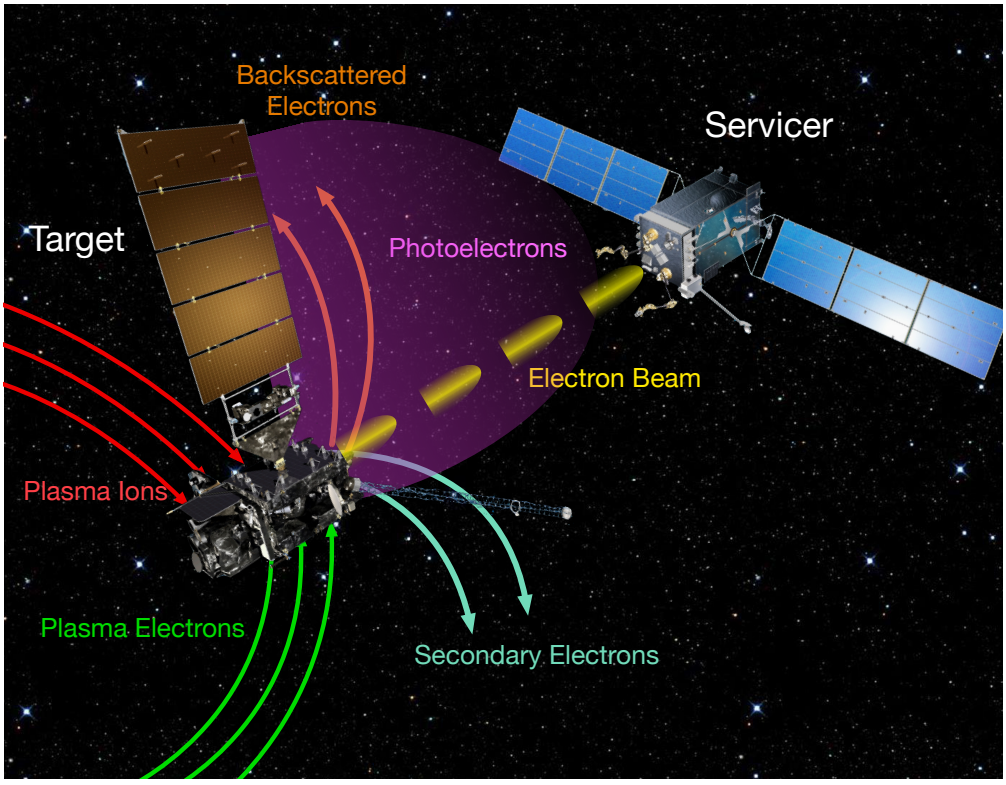


**Fig. 1 Conceptual representation of a satellite exposed to the space environment and an electron beam**

difference of target object and electron beam; comparing the measured x-ray energies and the electron beam energy yields the electric potential of the target[5, 6]. The servicing craft measures the energy spectrum of the electrons (or the photons depending on which method is being employed) and, knowing its own potential, determines the potential of the target object. When this is incorporated into the relative motion control of the spacecraft, these additional perturbations are accounted for, improving the performance of the controller and decreasing the possibility of a collision [3]. Both sensing methods have been experimentally validated for vacuum chamber conditions [7–10] in the Electrostatic Charging Laboratory for Interactions between Plasma and Spacecraft (ECLIPS) research vacuum chamber[11]. An electron beam is used to excite secondary electrons and x-rays from a small, usually aluminum, object used to represent a spacecraft. A Retarding Potential Analyser (RPA) measures the flux and energy of the secondary electrons and an x-ray detector is used to measure the energies of emitted x-ray photons[11]. The RPA is similar to a gridded Faraday cup where electrons with energy less than or equal to the potential across the grid can not pass through [11]. When sweeping through the energy spectrum, the grid potential that corresponds to a large drop off in measured current indicates the potential difference between the electron gun and the target. These experiments were conducted using a high voltage power supply (HVPS) to control the potential of the target object. While this is useful to test and validate remote sensing methods, the charge of a spacecraft is not always constant. Additionally, an electron beam applies a current to the target. Because the HVPS maintains a constant potential on the target, the charging effect due to the electron beam is eliminated.

A continuous beam of electrons applies an additional negative current that will alter the potential of the target. With a high energy electron beam, this can have a significant effect on the measured potential of the spacecraft: depending on the geomagnetic activity, the electron beam current can increase the magnitude of the target potential by kilo-volts[12]. This results in measurements that are not representative of the spacecraft environment. To reduce the effect, the energy and current of the electron beam could be adjusted such that the effect of the beam is minimal; however, there are limitations on how much these parameters can be changed and still be able to sense the target potential. Because of this, a different method for reducing this effect was proposed: using a pulsed beam rather than a continuous beam[12]. Figure 1 shows a conceptual representation of a servicing craft equipped with a pulsed beam. The electron gun used in the ECLIPS vacuum chamber is equipped with a grid across the aperture that, when a voltage is applied to it, keeps electrons from being emitted. This voltage can be oscillated, allowing the beam to pulse with a frequency up to 5 kHz.

While the beam is “on”, electrons are emitted and secondary electrons and x-rays can be measured. When the beam is off, the targets decreases to its natural potential. Simulations of a continuous electron beam and pulsed electron beam aimed at a target were conducted with a charging model that incorporates environmental and electron beam currents [12]. It was discovered that the potential of the target decreases while being sensed with an electron beam, especially when eclipsed[12]. Also, that by pulsing, the energy and current parameters of the beam can remain unchanged while the net current applied to the target is reduced.[12]

To explore this effect experimentally, an RC circuit was designed in previous work and attached outside the vacuum chamber, simulating the increased capacitance of a real spacecraft and the space environment[13]. A relationship between the RC circuit and the spacecraft charging model was developed such that the charging behavior of the circuit reflected that of the simulated spacecraft environment[13]. This allows for the transient charging behavior of the system to be measured for given environmental conditions. The external circuit is employed here to allow for more in-depth experiments for spacecraft charging. The goals of this paper include demonstrating that the secondary electron method yields accurate results with a pulsed electron beam as well as showing that using a pulsed beam reduces the electrostatic charging experienced by a target. The charging behaviors generated by continuous and pulsed beams is also compared in order to determine the effect beam parameters have on charging.

This paper is structured as an overview of the spacecraft charging model, experimental setup, and experimental results. The results explore sensing measurements yielded by a pulsed beam, a comparison between the charging behavior of target using the pulsed and continuous beam, and how the experimental charging results compare to the results of the spacecraft charging model.

## II. Materials and Methods

### A. Spacecraft Charging Model

While in the space environment, a satellite experiences a variety of different environmental currents. Regardless of orbit location, a spacecraft experiences an ambient electron and ion currents from impacting solar wind particles. Due to the large mass difference, electrons are significantly faster than ions, leading to a large negative current experienced by the spacecraft. A positive current is applied by the ambient ions, however it is typically less than that of the ambient electrons[1]. When an electron impacts the spacecraft surface, this "primary" electron may transfer some of their energy to the surface electrons. If enough energy is shared, one or more secondary electrons are emitted from the spacecraft[1]. Because there are electrons being removed, these secondary electron emissions (SEE) result in a positive current on the spacecraft. Sometimes, instead of being absorbed by the target, a primary electron is deflected the surface, generating a backscattered electron [1]. Unlike secondary electrons, the backscattered electron is the same as the impacting electron. While nothing is being removed from the spacecraft, this still results in a positive current. When calculating the ambient electron current, it is assumed that every electron impacts the spacecraft. Due to backscattered electrons, this is not necessarily true, so this additional positive current accounts for this assumption. In day-lit regions of an orbit, a photoelectron current is generated by high energy photons from the Sun. On the sun-facing side of the spacecraft, surface electrons are excited by these impacting photons and are consequently emitted from the craft with low energy[1]. If the satellite is charged negatively, these emitted electrons will be accelerated away, applying a positive current to craft[1]. However, if the spacecraft has a positive potential, these low energy electrons will be attracted back and a weak positive current will be experienced.

These currents are driven by the plasma temperature and density, lighting conditions, and the energy of impacting electrons, all of which vary between regions of space. When in sunlight, spacecraft typically charge weakly positive due to the dominating photoelectric current while objects in eclipsed geostationary orbits can charge to a few kilo-volts negative because of large ambient electron fluxes[1]. The potential of the spacecraft also affects the total current. A negatively charged spacecraft will attract ambient ions while repelling ambient electrons. Each natural current is modeled differently based on the sign of the spacecraft potential. While both are presented here, the experimental results use a negatively charged spacecraft. When the environmental currents are in equilibrium, the resulting potential is called the natural potential[1]. When an electron beam is applied to the object, an additional negative currents is generated. This current depends on the electron beam energy and current as well as a scaling parameter $\alpha$. Assuming an accurate and focused beam, the scaling parameter is equal to one[1]. With more impacting electrons, more secondary electron and backscattered electrons will be generated, meaning there is an SEE and backscattered electron current due to the electron beam as well.

This paper utilizes a charging model that simulates an electron beam current and the natural currents experienced

by a conducting spacecraft with spherical geometry. A model for secondary electrons and backscattered electrons is presented her, but to achieve a time invariant result, it is not considered in this paper.

The ambient electron current is

$$I_e(\phi) = -\frac{Aqn_e\omega_e}{4}e^{\phi/T_e} \qquad \phi < 0 \tag{1a}$$

$$I_e(\phi) = -\frac{Aqn_e\omega_e}{4}(1 + \frac{\phi}{T_e}) \qquad \phi \geq 0, \tag{1b}$$

where $n_e$, $T_e$, and $m_e$ are the electron density, temperature, and mass respectively, $\phi$ is the spacecraft potential, $A$ is the surface area exposed to the plasma, $q$ is the elementary charge, and $\omega_e = \sqrt{8T_e/\pi m_e}$ is the thermal velocity of electrons[14].

Similarly, the ambient ion current is

$$I_i(\phi) = \frac{Aqn_i\omega_i}{4}e^{-\phi/T_i} \qquad \phi > 0 \tag{2a}$$

$$I_i(\phi) = \frac{Aqn_i\omega_i}{4}(1 - \frac{\phi}{T_i}) \qquad \phi \leq 0. \tag{2b}$$

The variables are defined the same as in Eq. (1) except the subscript $i$ denotes ions[14]. An ion flux consisting of solely protons is assumed here.

Objects orbiting on the day-side of the earth experience the following photoelectron current from solar photons:

$$I_{ph}(\phi) = j_{ph,0}A_\perp e^{-\phi/T_{ph}} \qquad \phi > 0 \tag{3a}$$

$$I_{ph}(\phi) = j_{ph,0}A_\perp \qquad \phi \leq 0, \tag{3b}$$

with $A_\perp$ being the cross-sectional area exposed to the sunlight, $T_{ph} = 2$ eV being the temperature of emitted photoelectrons, and the photoelectron flux is assumed to be $j_{ph,0} = 20$ μA/m$^2$[1]. For negatively charged spacecraft, this emission is constant because the electrons will be repelled regardless of electron energy. However, for spacecraft with a positive potential, an electron with high enough energy relative to the spacecraft potential can escape, while the rest will be attracted back to the object.

When active, an electron beam applies a negative current to a target object. This current only occurs when the difference in electric potential between the servicer $\phi_S$ and the target $\phi_T$ is less than the initial energy $E_{EB}$ of the electron beam. When the difference is greater than or equal the electron beam energy, the emitted electrons do not have enough energy to reach the target and are repelled away. This is current is expressed by

$$I_T(\phi_T) = -\alpha I_{EB} \qquad \phi_S - \phi_T < E_{EB} \tag{4a}$$

$$I_T(\phi_T) = 0 \qquad \phi_S - \phi_T \geq E_{EB}, \tag{4b}$$

where $I_{EB}$ is the current of the electron beam and $\alpha$ is the fraction of the beam hitting the target. A value of $\alpha = 1$ is used, therefore an accurate and focused beam is assumed such that $I_T = -I_{EB}$ if the beam reaches the target.

Impacting low energy electrons and ions can cause the emission of secondary and backscattered electrons[1]. Reference 15 surveys various secondary electron emission models and demonstrates that different models yield significantly different results. The approximation developed in Ref. 16 where

$$I_{SEEB}(\phi_T) = -4Y_{\max}I_T(\phi)\kappa \qquad \phi < 0 \tag{5a}$$

$$I_{SEEB}(\phi_T) = 0 \qquad \phi \geq 0, \tag{5b}$$

with

$$\kappa = \frac{E_{\text{eff}}/E_{\max}}{(1 + E_{\text{eff}}/E_{\max})^2} \tag{6}$$

and

$$E_{\text{eff}} = E_{EB} - \phi_S + \phi_T \tag{7}$$

is used because it allows for a simple analytic expression of $I_{SEEB}$, with $E_{\text{eff}}$ being the effective energy of the beam electrons when they impact the target, $Y_{\max}$ being the maximum yield of electron emissions, and $E_{\max}$ being the landing energy at which the maximum yield occurs. As established by Ref. 17, the material properties for aluminum, $Y_{\max} = 2$

and $E_{max}$ = 300 eV, are used. The value for $Y_{max}$ includes both secondary and backscattered electrons. At energies greater than 1 keV, the yield can become negligible[1]. These material properties are for pure, clean aluminum; however the surfaces of metals can oxidize over time. A comparison of different aluminum secondary electron yield (SEY) data sets is conducted in Ref. 18. The average SEY for clean aluminum was 1.43 while the average yield for aluminum oxide was 2.83, suggesting that a coating of aluminum oxide can double the secondary electron yield[18].

Because these equations are used to represent the space environment, the natural potential can be calculated by setting the sum of the environmental currents to zero:

$$I_N(\phi_N) = I_{ph}(\phi_N) + I_i(\phi_N) + I_e(\phi_N) = 0. \tag{8}$$

Plasma density and temperature, driving factors of the ion and electron currents, differ significantly even in the same region of space: in geostationary orbits, plasma densities range from 0.1 - 1 $cm^3$[1]. In eclipsed regions, there is no photoelectron current and the plasma determines the natural potential. However, in sunlight regions, the photoelectron emission often dominates spacecraft charging[1]. This means a satellite that orbits in and out of eclipse can charge between a few kilo-volts negative to a few volts positive within the span of one orbit.

The electron beam applies additional currents, altering the potential of the spacecraft such that

$$I_{tot}(\phi) = I_{EB} + I_{SEEB}(\phi) + I_{ph}(\phi) + I_i(\phi) + I_e(\phi). \tag{9}$$

When the electron beam is on, the $I_{tot}$ determine how the object charges while, when the beam is off, only the natural currents affect the charging behavior as it returns to the floating potential.

An RC circuit is connected to the cube outside the vacuum chamber to simulate the environmental impact on a charged spacecraft. A relationship between the RC circuit and the spacecraft charging model was derived such that the circuit capacitance $C$ and resistance $R$, and floating potential $\phi_N$ are a function of the plasma and spacecraft properties[13]. These expressions were be found by relating the differential equation for voltage $\phi$ from the charging model and the experimental setup in the ECLIPS vacuum chamber[13].

When exposed to the space environment, the surface of the spacecraft charges based on the surface capacitance of the craft [1]. Because of this, an object in space can be simply modeled as a capacitor exposed to the same currents as the object. By reducing the problem to a capacitor and total current, the differential equation for a charging object is found using the equation of a capacitor and the sum of currents given by Eq. (9). At lower energies, around 300 eV, the secondary electron yield (SEY) of aluminum has a significant contribution to the overall potential[1]. The electron beam utilizes high energy electrons (above 3 keV), resulting in a low SEY. The current caused by the secondary electron emission is small relative to other currents so it is not included here. Also, in order to properly develop this relationship, $I_e$ was linearized about the natural potential $\phi_N$ using a first order Taylor expansion[13]. The sign of an object's potential determines the current experienced by the object shown by Eqs. (1) (2) (3). For these experiments, a negative potential is used; however the resulting equation is similar for a positively charged spacecraft. Combining Eqs. (2) (3), the linearized electron current, and the equation of a capacitor, the differential equation for the potential on a charging spacecraft is given by

$$C_{SC}\frac{\mathrm{d}\phi}{\mathrm{d}t} + \left(\frac{Aqn_i\omega_i}{4Ti} + \frac{Aqn_e\omega_e}{4Te}e^{\phi_N/T_e}\right)\phi = \frac{Aqn_i\omega_i}{4} + j_{ph,0}A_\perp - \frac{Aqn_e\omega_e}{4}e^{\phi_N/T_e}\left(1 - \frac{\phi_N}{T_e}\right) + I_{EB}, \tag{10}$$

where $C_{SC}$ is the surface capacitance of the spacecraft[13]. Note that the right hand side of the equation does not depend on $\phi_N$ and the left hand side is linear with respect to $\phi_N$.

Using Kirchhoff's Current Law around the $V_{in}$ node in Fig 3, the differential equation for voltage can be determined by balancing the currents into the node with the currents out of the node. Reorganizing the terms, the resulting relationship is

$$C\frac{\mathrm{d}\phi}{\mathrm{d}t} + \frac{1}{R}\phi = \frac{\phi_{N,RC}}{R} + i_{ext} + i_{EB}. \tag{11}$$

Here, $i_{ext}$ is an additional controlled current applied to the target that can simulate currents such as the photoelectron current or ion beam emission. These experiments do not include the photoelectron current, therefore $i_{ext}$ = 0. Because the circuit is connected directly to ground, the simulated natural potential of the circuit, $\phi_{N,RC}$ is also zero; $\phi_{N,RC}$ is equivalent to $\phi_N$.

By comparing the coefficients of Eq. (10) and Eq. (11), the relationship between the space environment and the components of the circuit was found to be

$$C = C_{SC}, \tag{12}$$

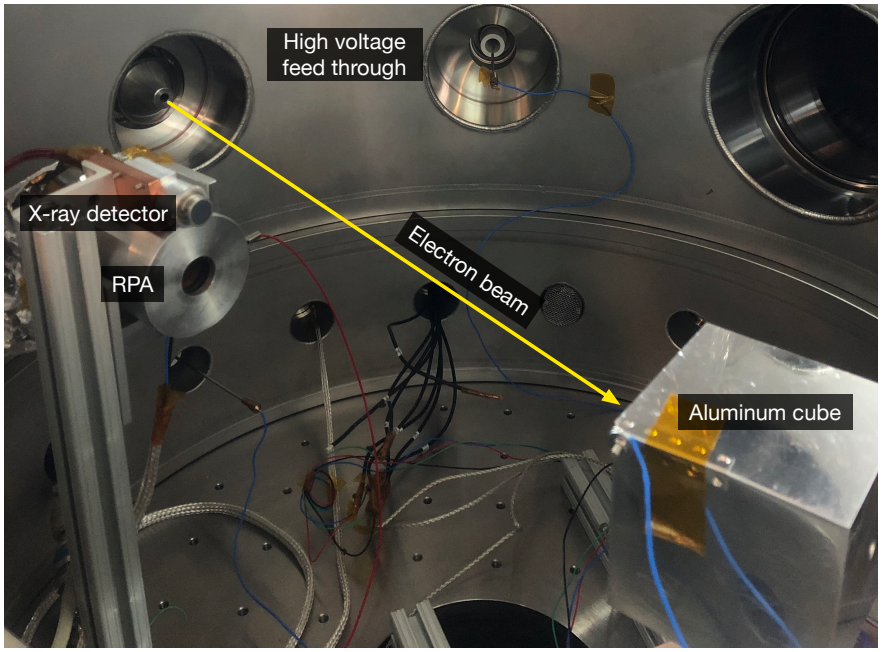


**Fig. 2 The experimental setup inside the ECLIPS vacuum chamber with a cube as the target object[11]**

$$R = \frac{1}{\frac{Aqn_i\omega_i}{4Ti} + \frac{Aqn_e\omega_e}{4}e^{\phi_N}}, \tag{13}$$

and

$$i_{ext} = \frac{Aqn_i\omega_i}{4} + j_{ph,0}A_{\perp} - \frac{Aqn_e\omega_e}{4}e^{\phi_N}(1 - \frac{\phi_N}{T_e}) - \frac{\phi_N}{R}. \tag{14}$$

The spacecraft capacitance is simply equal to the value of the circuit capacitor. Resistance and the external current, on the other hand, depend on the space weather conditions such as electron and ion density, ion temperature, and floating potential. A more detailed derivation of these equations is given in Ref. 13.

Reference 13 validates the relationship in Eqs. (12)(13)(14) by demonstrating that the discharging behavior of the experimental set up and the charging model are similar. It was found that, because of the linearized electron current, as the maximum potential of the cube deviates from the natural potential, these relationships begin to break down. For voltage magnitudes of 484 V or less, the circuit accurately simulated the effect the environment has on charging behaviors. For magnitudes greater than 1.562 keV however, the experimental results deviated significantly from the charging model.

### B. Experimental Setup

Experiments are conducted in the ECLIPS vacuum chamber with the hardware setup shown in Fig. 2. The experimental setup consists of a high energy electron gun, a 70 x 70 x 70 mm aluminum cube used to simulate the bus of a spacecraft, the RPA, and an additional RC circuit. The electron gun is a EMG-4212C from Kimball Physics capable of emitting electrons with currents ranging from 0.1 $\mu$A to 100 $\mu$A and with energies ranging from 0.1 keV to 30 keV. Before experiments are conducted, a 38 mm diameter Kimball Physics Rugged Phosphor Screen is used to ensure an accurate and focused beam. Blue light is emitted when electrons impact the screen, which is used to center the beam. Located outside the vacuum chamber, the circuit is connected to the spacecraft model by a high voltage feed-through. A diagram of the RC (resistor and capacitor) circuit used here as shown by Fig. 3 and Fig. 4 shows a picture of the actual circuit. In Fig. 4, the input of the circuit is connected to the high voltage feed through and the output is connected directly to the ground.

The goal of the circuit is to simulate the charging behavior of large spacecraft in the space environment. As the cube accumulates electrons, the charge flows out of the cube, in to the circuit. Adding the capacitor increases the overall capacitance to realistic values for spacecraft, slowing the rate of charging. Without this, the cube would charge to its

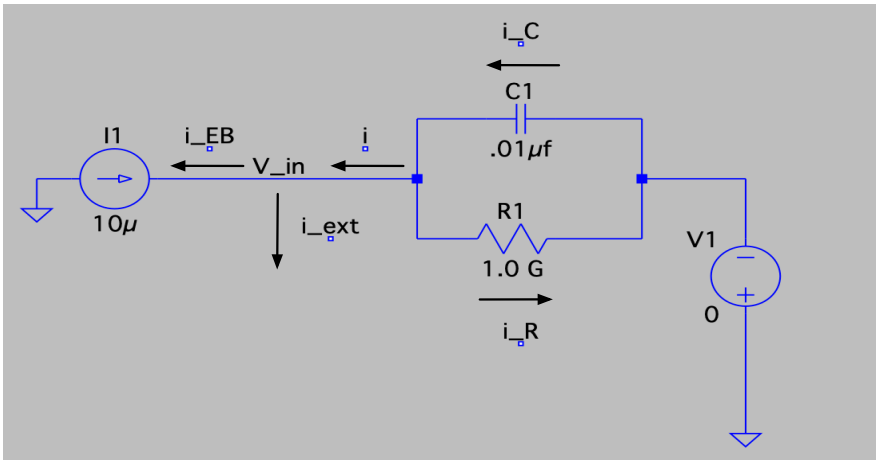


**Fig. 3 A schematic representative of the additional circuit connected to the target object**

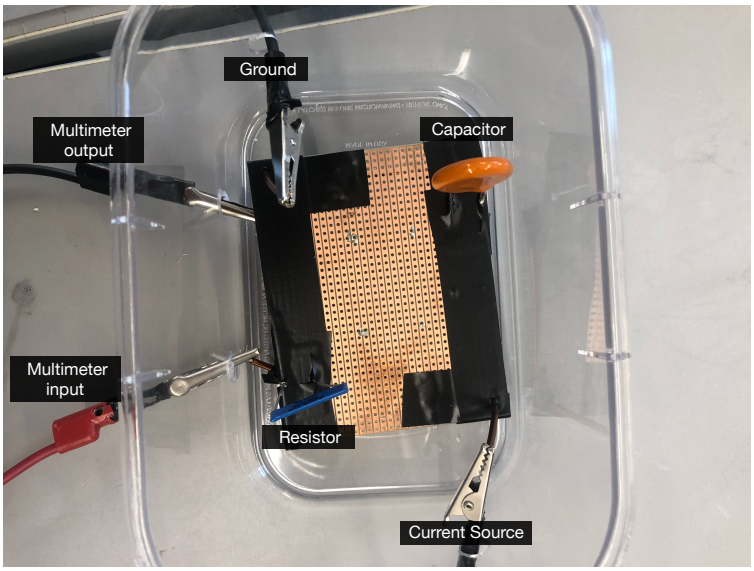


**Fig. 4 The RC circuit used in the experimental setup.**

steady state value instantaneous. With the addition of the resistor, the charging behavior of a given space environment can be simulated. When the electron beam is emitting, current flows from the cube into the capacitor and through the resistor. As the cube charges, the capacitor charges the same, allowing us to measure the charge behavior of the cube. While the electron beam is not impacting and the cube discharges, the current flows from the cube through circuit, replicating a spacecraft returning to its floating potential in the space environment. Increasing the capacitance extends the charging process, simulating the behavior of large spacecraft and allowing the charging behavior to be measured. The charging rate is also affected by the size of the resistor and the maximum voltage the capacitor can reach is determined by the resistor. To allow different environments to be simulated, the circuit is designed for the resistor and capacitor to be easily swapped out with components of varying sizes. Resistance values range from 100 MΩ to 1 GΩ while capacitance values vary from 100 pF to .01 µF.

The Kimball Physics EMG-4212C electron gun is capable of generating a pulsed beam through dual grid pulsing. Within the chamber of the electron gun, there is grid that, when a voltage is applied to it, electrons with insufficient energy can not penetrate through the gird. When no voltage is applied, the electrons exit the gun as normal. The grid cut off voltage is the minimum voltage that can be applied to the grid such that no electrons are emitted. For dual grid pulsing, there is one grid connected to two power supplies; one is the variable power supply while the other is set to the

grid cut off potential. A transistor-transistor-logic signal switches between the two supplies with a frequency between 1 Hz and 5 kHz. Beam pulse width can also be controlled and is limited to the period of the pulse. This means, while using the pulsing function of the beam, a continuous beam can not be achieved. The duty cycle, d, of the beam is the ratio of time the beam is on to the period of a pulse:

$$d = \frac{\text{Pulse Width}}{\text{Period}}. \tag{15}$$

To use the dual grid pulsing function, one must use the remote functions of the electron gun. A program through LabView is used to control every function of the electron including beam current, deflection, and grid potential. Along with being used for pulsing, the grid can be manually controlled, allowing for a continuous beam to be "turned off" with out changing beam parameters. This is important when transitioning between charging and discharging with the electron gun. Manual control of the grid is unavailable during pulsing, so to transfer between charging and discharging, the beam is deflected to the point where it no longer impacted the cube. The phosphorous screen is used to ensure this.

A Keithley Model DMM6500 6.5-Digit Multimeter is used as an amp-meter in series with the resistor and is capable of measuring currents as low as 10 pA. Although the potential across the capacitor is the desired measurement, the current through resistor is being measured. This is because the internal resistance of the multimeter is 10 MΩ, an order of magnitude less than the smallest resistor being used. Current flows through the path with the least resistance, therefore, when measuring voltage, it would flow through the multimeter yielding inaccurate results. Instead, current through the resistor is being measured, and using Ohm's law ($I = \phi/R$), the voltage across the resistor is calculated. Components in parallel have the same voltage, so this is also the voltage across the capacitor. A Matsusada AU-30R1 High-Voltage Power Supply is used to provide high quality potentials up to 30 kV with a maximum current of 1.0 mA.

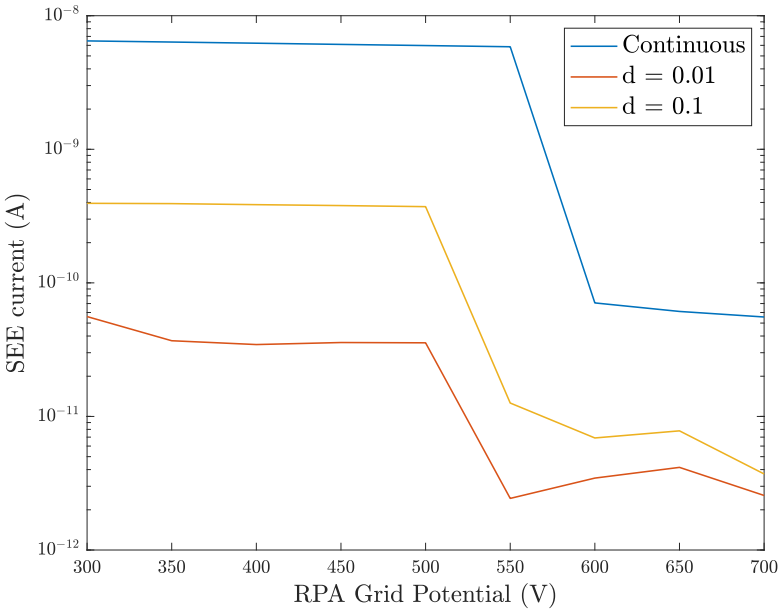


**Fig. 5 A continuous and pulsed beam with varying duty cycles is used to measure a cube with a −500 V potential. The x-axis shows the magnitude of the RPA Grid Potential; during experiments the grid potentials are negative.**

## III. Results

### A. Continuous Beam vs. Pulsed Beam

Employing a continuous electron beam to measure the electrostatic potential of a target object has been experimentally validated in the ECLIPS vacuum chamber[7, 8]. Similar experiments are conducted using a pulsed beam, specifically with the secondary electron method. The potential of a cube with a constant −500 V potential (achieved with the HVPS)

is measured by a 3000 V beam with a 3 $\mu$A current. Results from measuring the target potential with continuous beam and a pulsed beam with a duty cycle of 0.01 and 0.1 are shown in Figure 5.Because the pulsed beam is being treated as a continuous beam with a reduced current, the techniques for using secondary electron method did not have to be altered.

To determine the target potential, an RPA is used to measure the relative fluxes for the energies of secondary electrons by sweeping across a range of voltages. This results in "bins" of measurements for the relative secondary electron current for energies for some resolution. In this experiment, the range of voltages is $-300$ V to $-700$ V with a resolution of 50 V. Figure 5 shows that for both pulsed beams, there is a steep drop off in measured current at a grid potential of $-500$ V, indicating the potential of the target is between $-500$ V and $-550$ V. The continuous beam, on the other hand, shows a measured potential of $-550$ V. While this may appear to be an error, this means that the target potential is measured to be in the $-550$ V to $-600$ V bin. Each set of electron beam parameters yields a target potential of close to $-500$ V with the secondary electron method suggesting that the pulsed beam method is viable for measuring a target potential as long as the net current applied to the object is large compared to the background noise of the system.

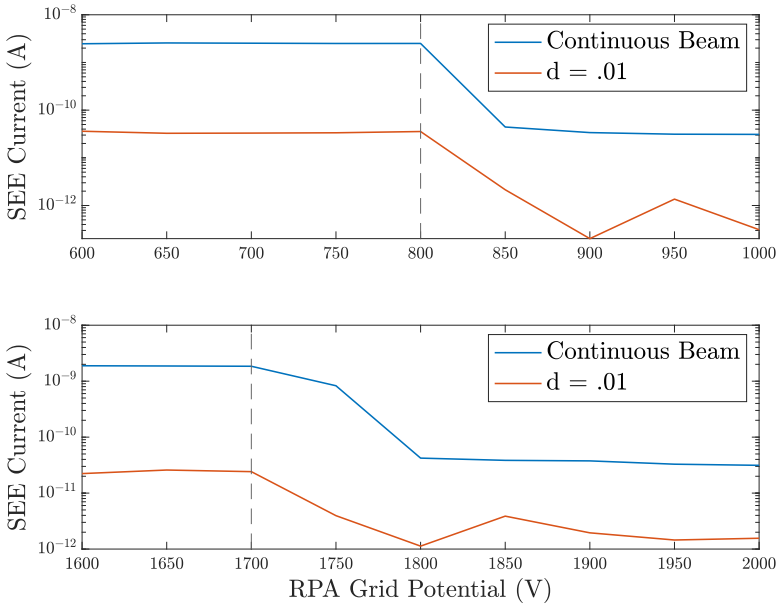


**Fig. 6 Floating Potential measurements for continuous and pulsed beams with varying energies. The x-axis shows the magnitude of the RPA grid potential and the y-axis is the relative SEE current.**

For the following experiment, the cube is disconnected from the HVPS and the circuit, meaning any current loss is from secondary electrons or self emitted electrons, allowing for the maximum potential that can be applied to the cube to be determined. The maximum potential occurs at the value where the ratio of electrons entering and leaving the cube is equal, therefore it is also the floating potential of the system. This ratio only depends on cube potential, therefore increasing/decreasing the current does not change the maximum potential. Because pulsing the beam should only decrease the net current applied to the cube, the floating potential for the pulsed beam and continuous beam should be the same. Figure 6 shows this potential found for a pulsed beam with a frequency of 1000 Hz and a 10 $\mu$s pulse width and a continuous beam. The cube is disconnected from the circuit so the secondary electron method is used to measure the target's potential. For beam energies of 5000 eV and 6000 eV, the pulsed beam and continuous beam both achieve floating potentials of $-800$ V and $-1700$ V respectively. The beam is pulsed with a frequency of 1000 Hz and a pulse width of 10 $\mu$s. With a duty cycle of .01, the net current applied to the cube is expected to be one hundredth the continuous: if the number of electrons impacting the cube is one hundred times less, then the secondary electrons would also be one hundred times less. This is seen in Figure 6 where the measured SEE currents are about $10^{-9}$ and $10^{-11}$ for the continuous and pulsed beams respectively.

These results suggests that the difference between the effect on the cube for a pulsed beam is the reduced net current: a pulsed beam with a duty cycle of .01 and a current of 3 $\mu$A should have the same response as a continuous beam with a .03 $\mu$A. Figure 7 compares the response from a pulsed beam to that of a continuous beam with the same net

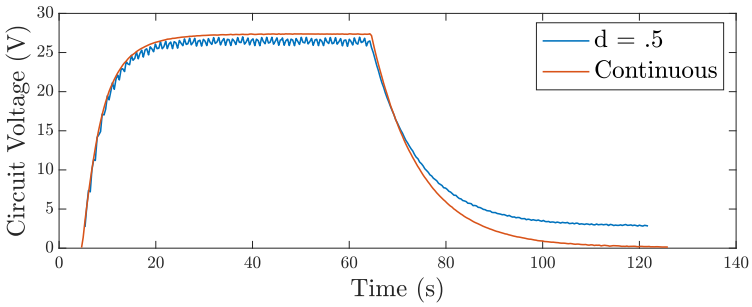


**Fig. 7 A comparison of the charging response to a pulsed beam with a current of 3 $\mu$A and duty cycle of .5 to a continuous beam with a current of 1.4 $\mu$A. The charging behavior for both beams is nearly identical while the discharging behavior, while similar, varies slightly.**

current. The beam is pulsed with a frequency of 1 Hz and a pulse width of .5 s. These parameters result in charging behavior that allows the actual pulses to be seen in the results; there is enough time while the beam is not emitting for the capacitor to noticeably discharge.

The main point of interest in this plot is the region between 4 and 60 s, where the beam is on and the cube is charging. Here, the behavior between both beams are nearly identical, except for the steady state voltage; however, they only deviate by about 1 V, likely due to inherent errors in the electron gun control. After 60 s, the beam is off and the circuit discharges so differences in beam parameters no longer effect the behavior. It is noticeable that pulsed beam and continuous beam do not discharge to the same value. This is because, while continuous beam can be fully turned off, the pulse beam can only be deflected off the cube due to limitations of the EMG-4212C electron gun control. Even though no electrons should be impacting the cube, some are, resulting in slightly non-zero potential. This experiment shows that a pulsed beam and continuous beam with the same net current yield the same charging behavior. A goal of this

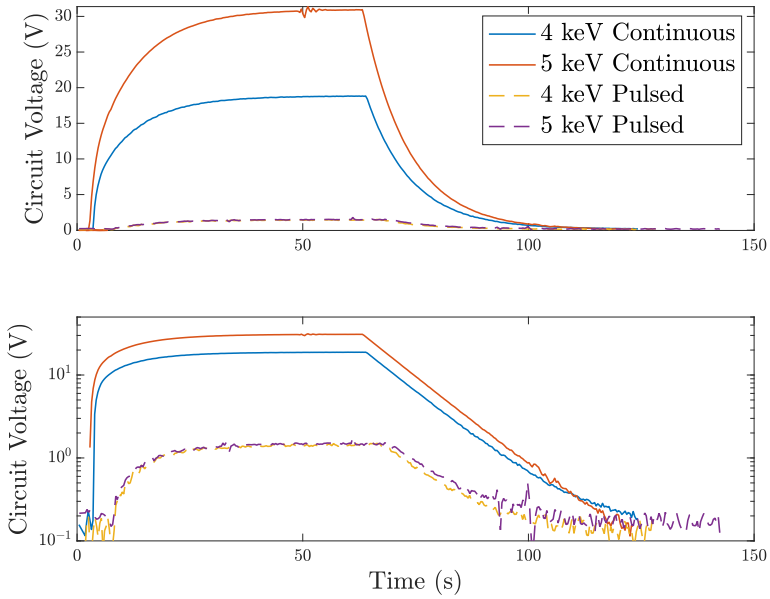


**Fig. 8 A comparison between a continuous and pulsed beam with 3 $\mu$A and energies of 4 keV and 5 keV. The beam is pulsed with a frequency of 1000 Hz and 10 $\mu$s pulse width. The values between the plots are the same; however, the bottom has log scale on the y axis. The y-axis shows the magnitude of the circuit voltage.**

paper is to show that implementing a pulsed beam instead of a continuous beam reduces the charging experienced by the

target object. While the energy varies, the beam current is held constant at 3 $\mu$A across all of the following experiments. Figure 8 has two plots: the top shows the voltage response of the circuit for a 3 $\mu$A continuous and pulsed beam with d = .01 for various energies while the bottom shows the same data with a log scale. It can be seen that for both energies, the pulsed beam applies a much lower voltage. For the continuous beam, the cube has a steady state potential of $-18.8$ V and $-30.1$ V for a 4 keV and 5 keV energy, respectively. On the other hand, the pulsed beam applies about $-1.8$ V for both beam energies. Because the pulsed beam has a duty cycle of .01, the net current is expected to be one hundredth of the continuous beam, resulting in one hundredth of the applied potential. These experimental results suggest that the pulsed beam actually applies a potential only one decade lower than the continuous beam. To explore this further, the beam energy is varied between 4 keV and 5 keV for the pulsed beam. Even with a significant variation in the beam energy, the maximum potential achieved is still $-1.8$ V, indicating that, for a pulsed beam with these parameters, the electron energy did not effect the potential applied to the cube. Together, these discoveries suggest that, with these parameters, the pulsed beam does not apply enough current to substantially charge the cube and can still be used to measure a target's potential.

### B. Experimental Results vs Simulations

Reference 13 shows that the discharging behavior of the circuit matches that of the spacecraft charging model. The discharging behavior is only dependent on the target potential and environmental parameters, suggesting that these currents are well represented by the RC circuit [13]. Figure 9 compares the charging behavior of a target object exposed to 4000 eV beam for the spacecraft charging and experimental data. There are multiple differences between the

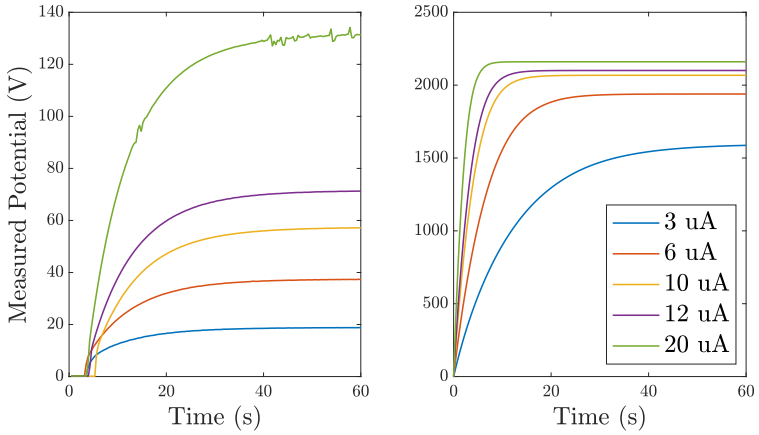


**Fig. 9 A comparison between a the experimental response of the circuit (Left) to the spacecraft charging model (Right) for a 4000 eV beam with varying currents. Similar results are achieved using a 5000 eV beam**

charging behaviors: the spacecraft model yields induced potentials much larger than the experimental data and the rate of charging varies as well. Because the discharging behavior was shown to match well [13], this suggests the error is in the modeled secondary and backscattered electron current. The model uses the beam energy and the secondary and backscattered electron yield curve for aluminum to determine the SEEB current. In the charging model, this is assumed to be the only electron loss from the system; however, the experimental setup may have multiple other losses including self-emittence from the cube or from various bare wires. Also, different secondary electron models have been shown to yield significantly different results[15]: the approximate SEE curve used in the model is likely not representative of the experimental setup. Before a realistic comparison can be made, the electron loss for this experimental setup must be characterized. The electron loss for a range of cube potentials will measured to generate a loss curve similar to a SEE yield curve. Because only the total current leaving the cube is needed, each loss current does not need to be characterized: the exact number of electrons lost due to self emittance is not necessary to measure, just the net current leaving the cube. Using this in the charging simulation to model a loss current instead of a secondary electron current should result in similar behavior between the experiments and spacecraft model.

## IV. Conclusions

This work explores the use of a pulsed beam for remote electric potential sensing, specifically the secondary electron method. The accuracy of measurements while pulsing is explored as well as a comparison between the charge transfer for a continuous and pulsed beam. Finally, the charging behavior caused by a continuous beam is compared to that of the spacecraft charging model.

While using the secondary electron method, a continuous beam and pulsed beam with varying duty cycles are applied to a target with a −500 V potential. Even with a duty cycle of d = 0.01, the pulsed beam yields accurate measurements of the target potential. The SEE current measured by the RPA is found to scale with duty cycle so, as the duty cycle decreases, noise will become significant enough to impact the results. An estimate of the noise would allow for a minimum duty cycle to be estimated. Floating potential experiments and charging behavior experiments with the additional circuit show that a pulsed beam acts as a continuous beam with a reduced net current: a 3 $\mu$A pulsed beam with a duty cycle of .5 has a similar effect on the target as a 1.5 $\mu$A continuous beam. The charging behavior of the circuit is measured with a continuous beam and a pulsed beam with a duty cycle of .01. It is shown that a pulsed beam does reduce the applied current while measuring the target potential; the current is low enough that it is likely there is not enough current to significantly charge the object for these conditions. This suggests that using a pulsed beam would be an effective method for reducing target charging while still yielding accurate results for the secondary electron method.

To verify the effectiveness of the circuit, the beam and environmental parameters are used in a charging model to simulate the charging behavior of a spacecraft. While previous research showed the environmental currents are accurately simulated by the circuit, the charging behavior and simulated behavior are found to not be similar. This is due to inaccurate modeling of the electron losses in the experimental setup. Future work will characterize the net current loss of the system due to secondary electrons, self emittance of the cube and exposed metal, and other un-modeled currents. Implementing the resulting loss curve in the spacecraft charging model will allow for a meaningful comparison between the experimental and simulated data.

## Acknowledgments

This work was supported by the U.S. Air Force Office of Scientific Research under grant FA9550-20-1-0025.

## References

[1] Lai, S. T., *Fundamentals of Spacecraft Charging*, Princeton University Press, 2011. https://doi.org/10.2307/j.ctvcm4j2n.

[2] Wilson, K., and Schaub, H., "Impact of Electrostatic Perturbations on Proximity Operations in High Earth Orbits," *Journal of Spacecraft and Rockets*, Vol. 58, No. 5, 2021, pp. 1–10. https://doi.org/10.2514/1.a35039.

[3] Wilson, K., Romero-Calvo, A., and Schaub, H., "Constrained Guidance for Spacecraft Proximity Operations Under Electrostatic Perturbations," *Journal of Spacecraft and Rockets*, 2022, pp. 1–13. https://doi.org/10.2514/1.A35162, in press.

[4] Ranvier, S., Anciaux, M., Cardoen, P., Gamby, E., Bonnewijn, I. S., De Keyser, J., Pieroux, D., and Lebreton, J. P., "Use of a Langmuir Probe Instrument on Board a Pico-Satellite," *IEEE Transactions on Plasma Science*, Vol. 45, No. 8, 2017, pp. 2007–2012. https://doi.org/10.1109/TPS.2017.2700211.

[5] Bengtson, M., Hughes, J., and Schaub, H., "Prospects and Challenges for Touchless Sensing of Spacecraft Electrostatic Potential Using Electrons," *IEEE Transactions on Plasma Science*, Vol. 47, No. 8, 2019, pp. 3673–3681. https://doi.org/10.1109/TPS.2019.2912057.

[6] Wilson, K., and Schaub, H., "X-Ray Spectroscopy for Electrostatic Potential and Material Determination of Space Objects," *IEEE Transactions on Plasma Science*, Vol. 47, No. 8, 2019, pp. 3858–3866. https://doi.org/10.1109/TPS.2019.2910576.

[7] Wilson, K. T., Bengtson, M. T., and Schaub, H., "X-ray Spectroscopic Determination of Electrostatic Potential and Material Composition for Spacecraft: Experimental Results," *Space Weather*, Vol. 18, No. 4, 2020, pp. 1–10. https://doi.org/10.1029/2019SW002342.

[8] Bengtson, M. T., Wilson, K. T., and Schaub, H., "Experimental Results of Electron Method for Remote Spacecraft Charge Sensing," *Space Weather*, Vol. 18, No. 3, 2020. https://doi.org/10.1029/2019SW002341.

[9] Bengtson, M., and Schaub, H., "Electron-Based Touchless Potential Sensing of Shape Primitives and Differentially-Charged Spacecraft," *AIAA Journal of Spacecraft and Rockets*, Vol. 58, No. 6, 2021, pp. 1847–1857. https://doi.org/10.2514/1.A35086.

[10] 'Alvaro Romero Calvo, Hammerl, J., and Schaub, H., "Touchless Potential Sensing of Differentially Charged Spacecraft Using Secondary Electrons," *Journal of Spacecraft and Rockets*, Vol. 59, No. 3, 2022, pp. 739–750. https://doi.org/10.2514/1.A35355.

[11] Wilson, K., Romero-Calvo, Á., Bengtson, M., Hammerl, J., Maxwell, J., and Schaub, H., "Development and characterization of the ECLIPS space environments simulation facility," *Acta Astronautica*, Vol. 194, 2022, pp. 48–58. https://doi.org/10.1016/j.actaastro.2021.12.037.

[12] Hammerl, J., and Schaub, H., "Using A Pulsed Electron Beam To Prevent Charging While Sensing Electric Potentials," *Applied Space Environments Conference*, 2021, pp. 1–17.

[13] III, J. D. W., Hammerl, J., and Schaub, H., "Design and Analysis for Experimental Validation of Touchless Charge Control Testing," *2022 AAS/AIAA Astrodynamics Specialist Conference*, Charlotte, NC, 2022.

[14] Hippler, R., Pfau, S., Schmidt, M., and Schoenbach, K. H., *Low Temperature Plasma Physics: Fundamental Aspects and Applications*, Wiley-VCH, 2001.

[15] Lundgreen, P., and Dennison, J., "Strategies for Determining Electron Yield Material Parameters for Spacecraft Charge Modeling," *Space Weather*, Vol. 18, No. 4, 2020. https://doi.org/https://doi.org/10.1029/2019SW002346.

[16] Draine, B., and Salpeter, E., "On the physics of dust grains in hot gas," *The Astrophysical Journal*, Vol. 231, 1979, pp. 77–94.

[17] Schaub, H., and Sternovsky, Z., "Active Space Debris Charging for Contactless Electrostatic Disposal Maneuvers," *Advances in Space Research*, Vol. 43, No. 1, 2014, pp. 110–118. https://doi.org/dx.doi.org/10.1016/j.asr.2013.10.003.

[18] Lundgreen, P., "The Development and Use of a Secondary Electron Yield Database for Spacecraft Charge Modeling," Master's thesis, 2020. https://doi.org/10.26076/90bd-5b32.

.